Steel and Composite Structures, *Vol. 34, No. 4 (2020) 547-559*
DOI: https://doi.org/10.12989/scs.2020.34.4.547

Prequalification of a set of buckling restrained braces: Part I - experimental tests

Aurel Stratan[1a], Ciprian Ionut Zub*[1] and Dan Dubina[1,2b]

[1]*Department of Steel Structures and Structural Mechanics, Politehnica University of Timisoara, Ioan Curea, no. 1, 300224, Timisoara, Romania*
[2]*Fundamental and Advanced Technical Research Centre, Romanian Academy, Timisoara Branch Bd. Mihai Viteazu, no. 24, 300223 Timisoara, Romania*

(*Received September 18, 2019, Revised January 14, 2020, Accepted January 18, 2020*)

Abstract. Buckling restrained braces (BRBs) were developed as an enhanced alternative to conventional braces by restraining their global buckling, thus allowing development of a stable quasi-symmetric hysteretic response. A wider adoption of buckling restrained braced frames is precluded due to proprietary character of most BRBs and the code requirement for experimental qualification. To overcome these problems, BRBs with capacities corresponding to typical steel multi-storey buildings in Romania were developed and experimentally tested in view of prequalification. The first part of this paper presents the results of the experimental program which included sub-assemblage tests on ten full-scale BRBs and uniaxial tests on components materials (steel and concrete). Two different solutions of the core were investigated: milled from a plate and fabricated from a square steel profile. The strength of the buckling restraining mechanism was also investigated. The influence of gravity loading on the unsymmetrical deformations in the two plastic segments of the core was assessed, and the response of the bolted connections was evaluated. The cyclic response of BRBs was evaluated with respect to a set of performance parameters, and recommendations for design were given.

Keywords: buckling restrained brace; experimental testing; prequalification

1. Introduction

Seismic design of most steel structures takes benefit of dissipation of part of the seismic energy through cyclic yielding in the ductile components of the structural system. Concentrically braced steel frames are often adopted due to their large strength and stiffness. However, buckling of braces limits to a certain extent the potential of steel in providing a ductile response. Buckling restrained braces (BRBs) were developed as an enhanced alternative to conventional braces by restraining their global buckling, allowing development of a quasi-symmetric and stable hysteretic response.

Since the development of this pioneering concept by Yoshino et al. in the 1970's, as shown by Xie (2005), BRBs were extensively studied worldwide. A comprehensive review of past research on buckling restrained braces is available in Uang *et al.* (2004), Xie (2005), Della Corte *et al.* (2011), Tsai *et al.* (2013), Takeuchi and Wada (2017).

Most of the BRBs developed to date are proprietary, but their principle of operation is similar (Uang *et al.* 2004). A typical BRB consist of a steel core encased in a steel tube filled with mortar or concrete. A layer of unbonding material or a small air gap is provided between the steel core and the mortar in order to minimise the transfer of axial forces from the steel core to the mortar and steel tube during elongation and contraction of the steel core, and also allows for its expansion when in compression (Black *et al.* 2002, Clark *et al.* 1999).

Buckling restrained braces constructed of all-steel components have been proposed as an alternative to mortar-filled steel tubes (Tinker and Dusicka 2012). Benefits of all-steel BRBs have been explained as lightweight (Usami *et al.* 2012), less expensive and easier to construct (Tremblay *et al.* 2006), having replaceable cores (Chou and Chen 2009), detachable (D'Aniello *et al.* 2014) or compact for installation in existing building walls (Della Corte *et al.* 2015).

Some countries introduced BRBs in their design codes: Japan, USA, Canada, Taiwan (Xie 2005). In Europe, the use of BRBs is not regulated by EN 1998-1 (2004) yet, but requirements regarding testing and manufacturing of BRBs are available in EN 15129 (2010). On the other hand, starting with January 2014, seismic design provisions for steel buckling-restrained braced frames are available in the Romanian national seismic design code P100-1/2013 (2014). The code requires experimental qualification of BRBs used in practical applications, either project-specific or based on existing experimental evidence. Recently, Vigh *et al.* (2017) proposed a design approach for buckling-restrained braced frames conforming to Eurocodes.

*Corresponding author, Ph.D.
E-mail: ciprian.zub@student.upt.ro
[a]Associate Professor
[b]Professor

ISSN: 1229-9367 (Print), 1598-6233 (Online)

Table 1 Geometry of BRB specimens (measured dimensions, mm)

Type	ID	Plastic zone				Tr. z.	Elastic zone						BRM			BRB
		t_{pl}	h_{pl}	L_{pl}	L_s	L_{tr}	t_{el}	h_{el}	L_{el}	t_{stf}	w_{stf}	L_{stf}	D_e	t	L_{BRM}	L_{BRB}
A	CR33-1	14.39	60.29	2532	60	90	14.39	150	609	13.8	69	565	168.33	3.71	3652	3930
	CR33-2	14.38	60.33	2532	60	90	14.38	150	609	13.8	69	565	168.47	3.74	3652	
	CR71-1	20.35	99.12	2478	100	65	20.35	164	661	20.1	71	609	177.97	3.97	3628	
	CR71-2	20.22	99.25	2478	100	65	20.22	164	661	20.1	71	609	178.07	4.04	3628	
	CR73-1	19.95	99.09	2462	100	73	19.95	172	661	20.1	75	614	193.80	5.99	3628	
	CR73-2	20.33	99.08	2462	100	73	20.33	172	661	20.1	75	614	193.87	6.01	3628	
B	CS33-1	30.11	30.22	2778	14	65	15.32	150	576	7.6	68	546	168.90	3.71	3648	
	CS33-2	30.16	30.28	2778	14	65	15.11	150	576	7.6	68	546	168.77	3.79	3648	
	CS73-1	44.80	44.75	2638	20	65	22.02	172	646	13.9	52	606	193.65	6.00	3628	
	CS73-2	44.82	44.73	2638	20	65	22.01	172	646	13.9	52	606	193.77	5.96	3628	

As project-specific qualification is time-consuming, several BRBs were developed and experimentally tested in view of prequalification. The capacity of the specimens (300 kN and 700 kN) corresponds to typical low-rise and mid-rise multi-storey buildings in Romania (Stratan *et al.* 2015). Considering the specifications from ANSI/AISC 341-10 (2010) regarding the similarity between the test specimen and prototype, the strength range covered by the two BRB capacities is 150-840 kN. The experimental qualification was done based on P100-1/2013 (2014) and ANSI/AISC 341-10 (2010) provisions.

Initially, conventional (BRBs consisting of a steel core encased in a steel tube filled with concrete) and all-steel BRBs were investigated numerically (Zub *et al.* 2018a) and experimentally (Stratan *et al.* 2018). Based on the performance of tested specimens and the technic and economic aspects, it was concluded that the optimal solution is the conventional BRB consisting of a steel core encased in a steel tube filled with concrete.

This paper presents the results of the experimental program which includes sub-assemblage tests on ten full-scale BRBs and uniaxial tests on base materials (steel and concrete). These results are the basis for developing a complex nonlinear numerical model of the buckling restrained brace using the finite element environment Abaqus (Dassault 2014), which are discussed in a companion paper (Zub *et al.* in press).

2. BRB typologies

The dissipative component of a BRB is a variable cross-section steel core consisting of several segments (connection, elastic, transition and plastic), see Fig. 2 which carries the axial load. The core is placed in a buckling restraining mechanism that prevents its global buckling (Uang *et al.* 2004). The two components are decoupled by an unbonding interface (material or gap), thus allowing the core to achieve higher compression modes (Sridhara 1990).

Two BRB typologies were investigated: type A and type B (Fig. 2). The core of the BRB of type A is milled from a steel plate, which assures a smooth transition from the plastic (L_p) to the elastic (L_e) region. The elastic cross-section section consists of the enlarged core segment (of height h_e, thickness t_e, and length L_e) and the two stiffeners (of width w_{stf}, thickness t_{stf}, and length L_{stf}). The main role of the elastic zone is to allow sliding of the core ends with respect to the buckling restraining mechanism, without excessive rotation, so that the BRB behaves essentially axially. Stiffeners are missing over a short length ($2t_{el}$) of the elastic zone, in order to limit the bending moment transmitted to the BRB ends due to the frame effect to the value of the plastic moment of the cross-section in the "$2t_{el}$" zone.

The core of the BRB of type B is fabricated from compact hot-rolled square steel profile, while the elastic zone is obtained by welding core extension plates and stiffeners to each end of the core.

The transition zone (of length L_{tr} and radius R_t) is an intermediate segment between the plastic and elastic zones and needs a careful design and fabrication to prevent stress concentrations and brittle failure modes. The plastic zone (of height h_p, thickness t_p, and length L_p) is split into two segments due to the presence of the stopper (of length L_s, radius R_s, and height h_s), which prevents free sliding of the BRM with respect to the core under cyclic loading. A gap (polystyrene foam) of length L_G = 70 mm is provided in the extension of the transition zone and stiffeners to allow for free movement under compression cycles.

Core to concrete gaps in the through-thickness (g_t) and the through-width (g_w) directions are obtained by wrapping the core with an acrylic tape. All BRB specimens have the same length between the gussets L_{BRB}. The measured geometrical characteristics of the BRBs specimens are presented in Table 1.

The buckling restraining mechanism (BRM) is a concrete-filled steel tube with exterior diameter D_e and wall thickness t. The unbonding material is a self-adhesive acrylic tape. Different lengths, L_{BRM}, resulted due to

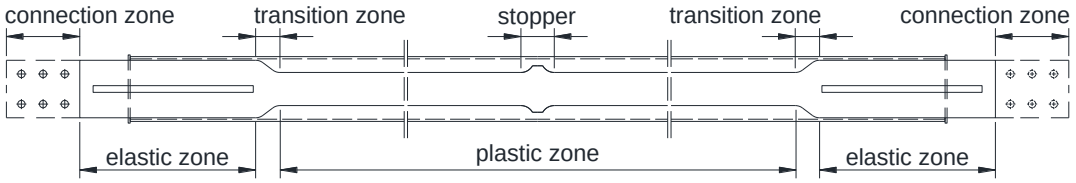

Fig. 1 Segments of a BRB core

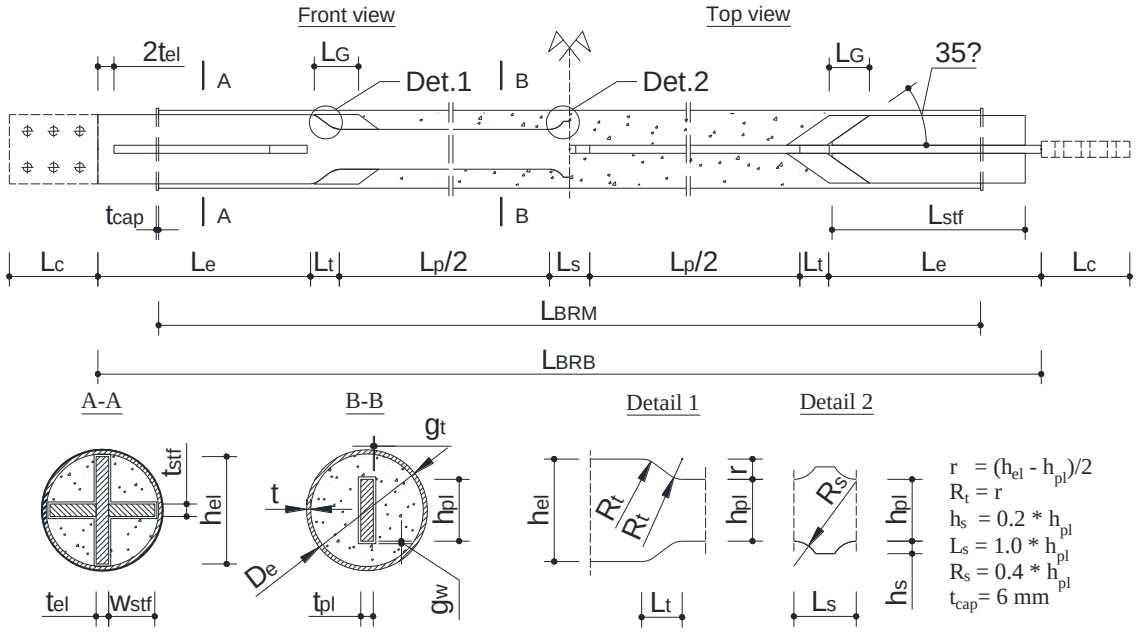

(a) BRB Type A: specimens CR33, CR71, CR73

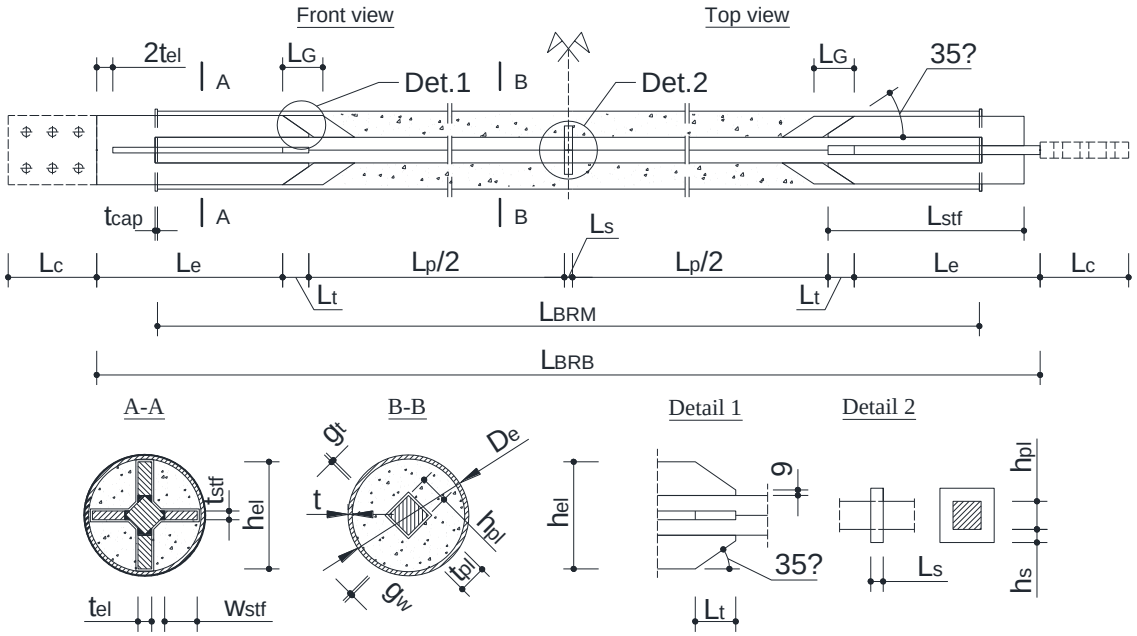

(b) BRB type B: specimens CS33, CS73

Fig. 2 The conceptual geometry of the tested BRBs

different geometrical configurations of the core. The steel tubes were infilled with concrete obtained from ready-mix cement mortar and 4-8 mm aggregates.

3. Experimental program

The experimental program is summarized in Table 2 and consists of ten BRBs. Two identical specimens were

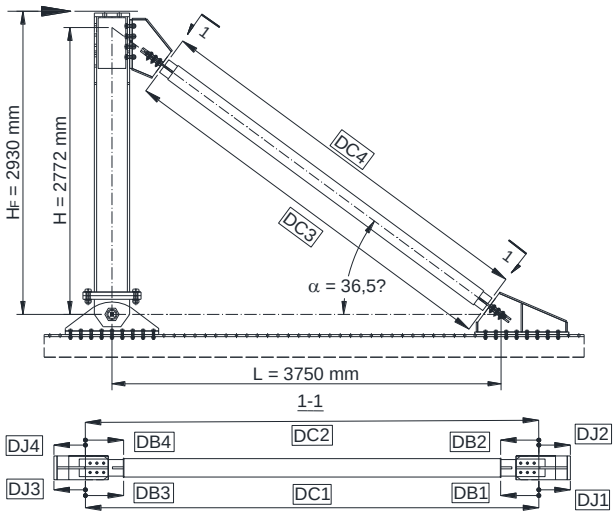

Fig. 3 Experimental test setup and instrumentation

fabricated for each distinct BRB solution. The core of all specimens was fabricated from S355 steel grade. The nominal size of the core of BRBs of types A was 14x60 mm for the 300 kN specimens, and 20x99 mm for the 700 kN specimens. In the case of the type B specimens, the core was fabricated from squares of 30x30 mm and 45x45 mm, for 300 kN and 700 kN capacities, respectively.

Early studies on bucking-restrained braces suggested that to prevent global buckling of the BRB, the elastic critical force N_{cr} of the bucking-restraining mechanism (BRM) be at least 1.5 times the nominal resistance of the core N_p (Watanabe *et al.* 1988). However, some studies (Iwata and Murai 2006) suggested that $N_{cr}/N_p \geq 3$ is necessary to obtain cumulative inelastic deformations in excess of 200 times the yield deformation, as required by ANSI/AISC 341-10 (2010). To assess the influence of the BRM design approach, two specimens (CR71-1 and CR71-2) were designed for $N_{cr}/N_p = 1.5$, while all the others for $N_{cr}/N_p \geq 3$. The value of N_{cr} was computed based on the recommendations from Iwata and Murai (2006)

$$N_{cr} = \pi^2 E_s \left(I_s + \frac{I_c}{20} \right) / L_{cr}^2 \quad (1)$$

where $E_s = 210000$ MPa is the elastic modulus of steel, I_s and I_c are the moments of inertia of the steel tube and the concrete cross section, respectively, L_{cr} is the buckling length of the BRM, assumed equal to the length of the BRB, as the "$2t_{el}$" zone (see Fig. 2) are relatively flexible with respect to the connection zone.

The thickness of the unbonding layer was adjusted depending on the shape of the core and capacity of the BRBs. Thus, a uniform 2 mm acrylic tape was applied on the cores of the BRBs of type B (square cross-section) and of the 300 kN type A (rectangular cross-section). A nonuniform thickness configuration (2 mm for the through-thickness direction, g_t, and 3 mm for the through-width, g_w, direction) was adopted in the case of the 700 kN BRBs of type A (rectangular cross-section). Gap size is an important parameter affecting the BRB performance (D'Aniello *et al.* 2014, Pandikkadavath and Sahoo 2016). To establish the optimum gap size for the BRBs described in this study, a parametric numerical simulation was carried out (Zub *et al.* 2018b).

4. Experimental setup and instrumentation

The experimental setup presented in Fig. 3 consists of a BRB-column sub-assemblage, loaded by a horizontal force at the column tip in displacement control. This loading set-up reproduces the frame effect, which induces bending moments on the BRB ends due to lateral drifts, as required by ANSI/AISC 341-10 (2010). Out of plane displacements were restrained at the top of the column.

The ANSI/AISC 341-10 (2010) loading protocol was used (Fig. 4), up to the attainment of a deformation in the BRB corresponding to twice the design inter-storey drift ($2\Delta_{bm}$). It consists of 2 cycles at each of the following amplitudes: Δ_{by}, $0.5\Delta_{bm}$, $1.0\Delta_{bm}$, $1.5\Delta_{bm}$, $2.0\Delta_{bm}$, where Δ_{by} is the yield deformation of the BRB. Since the condition of attaining a minimum cumulative inelastic deformation of 200 times the yield deformation was guaranteed by this loading sequence, in a second step, the loading was continued with 2 cycles at $2.5\Delta_{bm}$, followed by cycles at $1.5\Delta_{bm}$ until failure was attained. The cycles at $2.5\Delta_{bm}$ were additionally introduced to check if the proposed BRB typologies can develop even larger plastic deformations then $2.0\Delta_{bm}$. Where duplicate BRB specimens existed, the first specimen was loaded starting the protocol in tension (*T*) and the second specimen was loaded starting the protocol in compression (*C*), see Table 2.

The design inter-storey drift at the ultimate limit state in the seismic design combination was assumed equal to 2% of the storey height, according to P100-1/2013 (2014). The storey height in the archetype structures (Stratan *et al.* 2015) was 3500 mm, which led to a design inter-storey drift of 70 mm.

Table 2 Experimental program

Type	ID	A_p mm^2	N_p kN	N_{cr} kN	N_{cr}/N_p	Loading protocol	Unbonding material	Gaps, mm g_t	Gaps, mm g_w
A	CR33-1	867.6	345.1	873	2.53	*T*	acrylic tape	2	2
	CR33-2	867.5	345.1	881	2.55	*C*	acrylic tape	2	2
	CR71-1	2017.1	724.3	1103	1.52	*T*	acrylic tape	2	3
	CR71-2	2006.8	720.7	1123	1.56	*C*	acrylic tape	2	3
	CR73-1	1976.8	709.5	2093	2.95	*T*	acrylic tape	2	3
	CR73-2	2014.3	722.9	2102	2.91	*C*	acrylic tape	2	3
B	CS33-1	909.9	331.3	882	2.66	*T*	acrylic tape	2	2
	CS33-2	913.2	332.5	897	2.70	*C*	acrylic tape	2	2
	CS73-1	2004.8	565.0	2091	3.70	*T*	acrylic tape	2	2
	CS73-2	2004.8	565.0	2083	3.69	*C*	acrylic tape	2	2

A_p – area of the plastic zone of the core computed using mean values of the measured dimensions.
N_p – plastic resistance of the core computed using A_p and the mean yield strength of the steel of the core, R_{eH} (see Table 3)

The corresponding BRB deformation was 51 mm. Deformation of the BRB core (D_c) was obtained as the average of four displacement transducers (*DC*1…*DC*4) and was used as the control displacement

$$D_c = (DC1 + DC2 + DC3 + DC4)/4 \quad (2)$$

Displacement of the bottom core end with respect to the BRM (D_{bb}) was measured with transducers *DB*1 and *DB*2. Similarly, displacement of the top core end with respect to the BRM (D_{bt}) was measured with transducers *DB*3 and *DB*4:

$$D_{bb} = (DB1 + DB2)/2 \quad (3)$$

$$D_{bt} = (DB3 + DB4)/2 \quad (4)$$

Transducers *DJ*1…*DJ*4 were used to monitor connection deformations. Displacement of the bottom core end with respect to the bottom gusset (D_{jb}) was measured with transducers *DJ*1 and *DJ*2. Similarly, displacement of the top core end with respect to the top gusset (D_{jt}) was measured with transducers *DJ*3 and *DJ*4

$$D_{jb} = (DJ1 + DJ2)/2 \quad (5)$$

$$D_{jt} = (DJ3 + DJ4)/2 \quad (6)$$

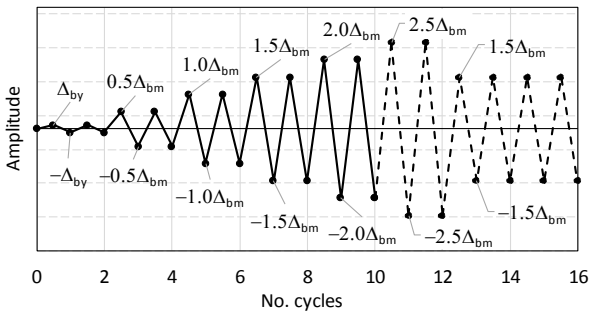

Fig. 4 Loading protocol used for experimental tests

5. Tests on component materials

Uniaxial tensile tests were performed to determine the mechanical properties of steel used to manufacture the core of the BRBs. Three coupons were extracted parallel with the rolling direction from each of the plates/squares used tofabricate the cores. The mean values of the mechanical characteristics obtained are summarized in Table 3: upper yield strength (R_{eH}), tensile strength (R_m), percentage elongation after fracture (A), over-strength factor of the material (γ_{ov}), defined as the ratio between the measured and nominal values of upper yield strength. All the tensile tests results comply with the product standard except for the C45 material.

Five more tests for assessment of cyclic response of steel were performed on short coupons extracted from the material used in fabrication of the core of the CS33 BRBs. The coupons were turned to the dimeter d_0 of 14 mm and the initial gauge length ($L_0 = d_0$).

Specimen C30-m was tested monotonically to provide data related to the yield strength, the strain at the end of the plateau, ultimate strength and its corresponding strain. The other specimens were tested cyclically at constant strains of 1.4% (C30-1.4%), 3.0% (C30-3.0%) and 5.0% (C30-5.0%), respectively. The last specimen, C30-var, was tested cyclically at variable strain amplitudes of ±1%, ±3%, ±5%, ±7%, and continued with cycles at ±5% until failure occurred. The stress-strain curves obtained under monotonic and cyclic loading are shown Fig. 5.

To evaluate the uniaxial compression strength of the concrete used in BRBs, six 150x150x150 mm cube specimens were tested. Three specimens were cured in water to assure the standard conditions for testing, while the other three specimens were cured in room conditions (similar to the ones that the BRBs are usually exposed to). Slightly larger (7%) averaged compression strength was recorded for the specimens cured in water ($f^w_{c,cube}$ = 50.5 N/mm^2) with respect to the ones in room conditions ($f^a_{c,cube}$ = 47.3 N/mm^2).

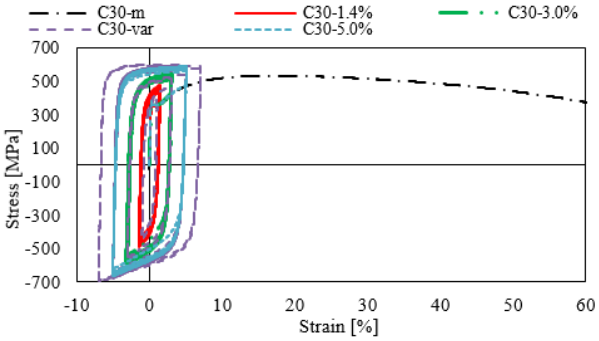

Fig. 5 Stress-strain results on cyclic material tests

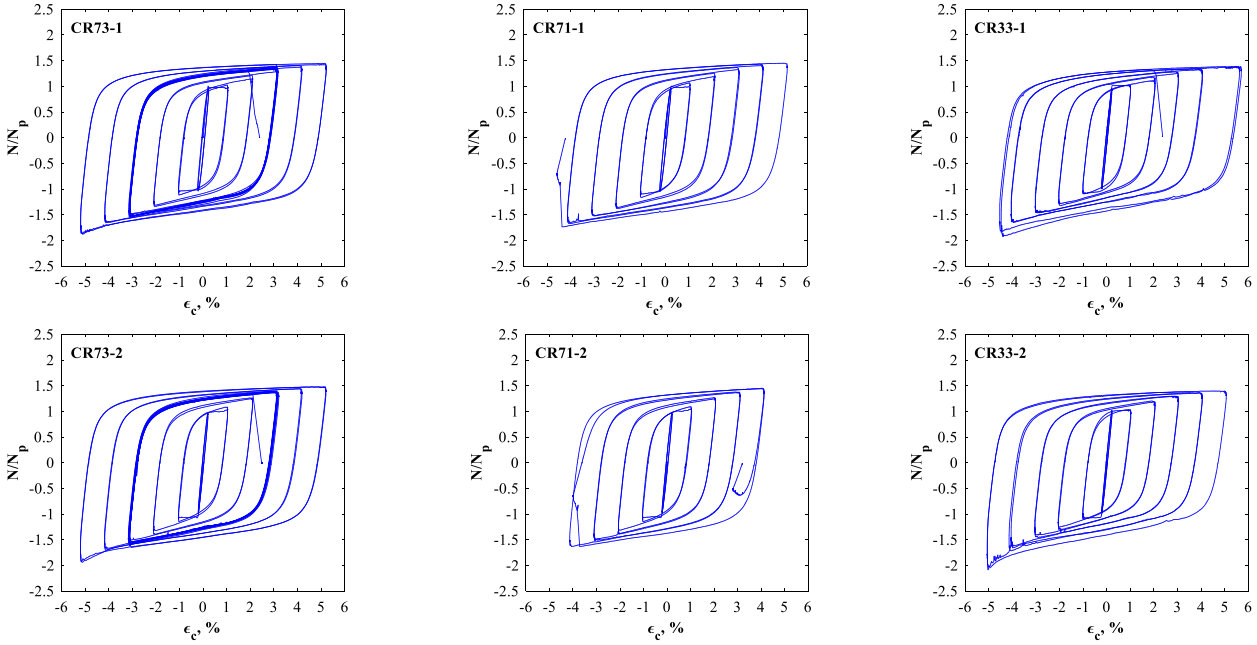

Fig. 6 Cyclic response of BRBs type A

Table 3 Mechanical properties of steel components

Material ID	Used in BRB	Product standard			Quality certificate			Tensile test				γ_{ov}
		R_{eH} (min) N/mm²	R_m N/mm²	A %	R_{eH} N/mm²	R_m N/mm²	A %	R_{eH} N/mm²	$R_{p0.2}$ N/mm²	R_m N/mm²	A %	
C14	CR33	355	470-630	22	N/A	N/A	N/A	398	395	513	36.2	1.12
C20	CR71, CR73	345	470-630	22	358	508	33.1	359	349	510	34.7	1.04
C30	CS33	345	470-630	22	384	600	25.4	364	354	525	30.6	1.06
C45	CS73	335	470-630	21	353	498	30.0	282	278	442	35.3	0.84

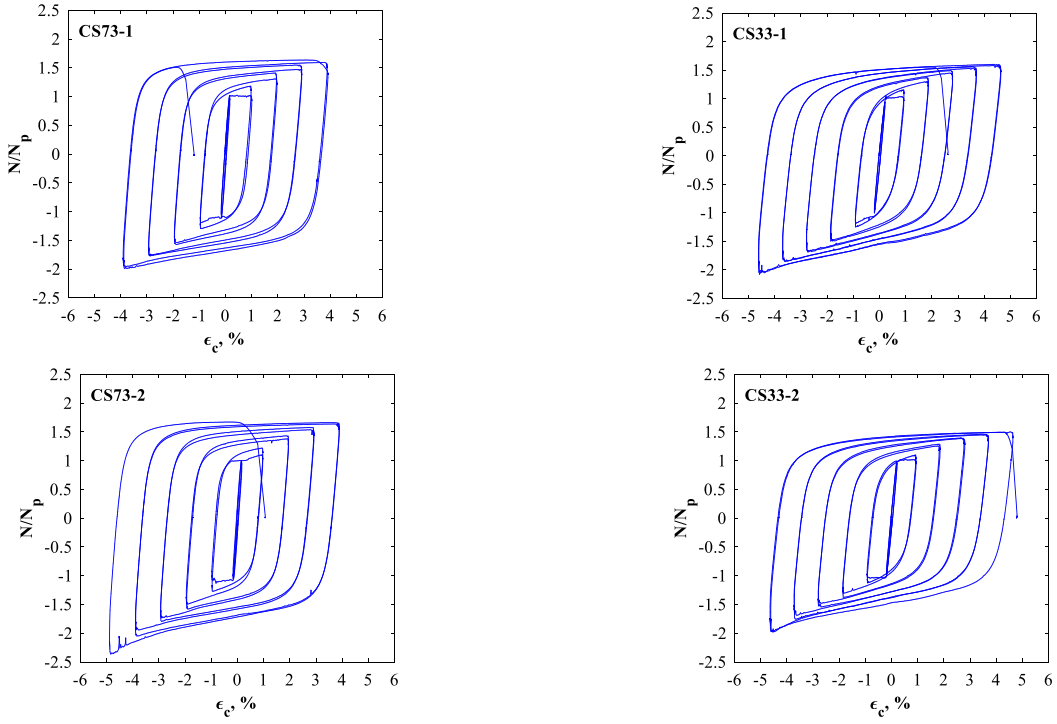

Fig. 7 Cyclic response of BRBs type B

(a) Front view (b) Side view (c) BRB-to-gusset lower connection view

Fig. 8 Failure mode of BRBs designed for $N_{cr}/N_p = 3.0$

6. Tests on BRB sub-assemblies

6.1 Cyclic response

The cyclic response of the tested BRBs in terms of normalized axial force (N/N_p) and core axial strain ($\varepsilon_c = D_c/L_p$) is presented in Figs. 6 and 7. In almost all cases, the response is stable and quasi-symmetric during the prequalification loading protocol.

6.2 Performance parameters

Performance parameters of the tested BRBs are summarized in Table 4. All BRB specimens developed a cumulative inelastic deformation, *CID*, greater than 200 times the yield deformation, Δ_{by}. Only 8 out of 10 BRBs could sustain the entire prequalification loading protocol (10 cycles up to $2\Delta_{bm}$). The compression strength adjustment factor, β, is defined as (Fig. 9)

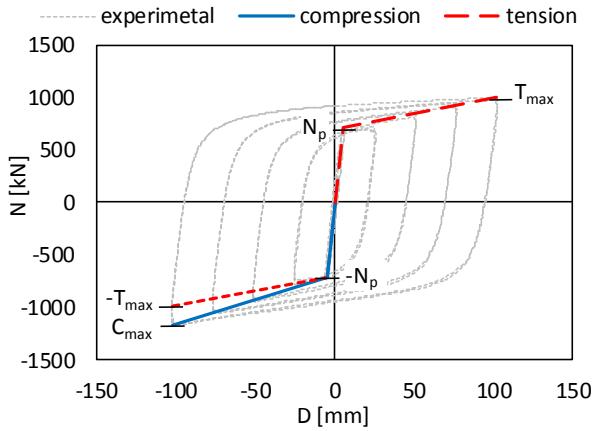

Fig. 9 Forces characterising the response of a BRB

Table 4 Summary of performance parameters

ID	Qualification protocol				Extended protocol				No. of cycles to failure
	ω	$\omega\beta$	ε_c, %	CID/Δ_{by}	ω	$\omega\beta$	ε_c, %	CID/Δ_{by}	
CR33-1	1.35	1.65	4.05	334.4	1.39	1.92	4.53	509.6	12.0
CR33-2	1.37	1.66	4.04	334.4	1.40	2.09	5.06	465.8	11.5
CR71-1	1.43	1.65	4.14	354.8	1.45	1.74	4.59	401.2	10.5
CR71-2	1.45	1.63	4.13	281.5	-	-	-	-	9.0
CR73-1	1.40	1.64	4.16	358.8	1.45	1.88	5.19	1256.3	25.0
CR73-2	1.44	1.70	4.17	358.8	1.48	1.94	5.20	1283.7	25.5
CS33-1	1.56	1.85	3.69	348.5	1.60	2.08	4.62	530.7	12.0
CS33-2	1.46	1.76	3.70	348.5	1.50	1.98	4.64	507.9	11.75
CS73-1	1.64	1.99	3.90	435.3	-	-	-	-	9.75
CS73-2	1.66	2.05	3.88	458.9	1.67	2.36	3.88	518.3	10.5

$$\beta = C_{max}/T_{max} \quad (7)$$

where C_{max} is the maximum compression force and T_{max} is the maximum tensile force.

The strain hardening adjustment factor, ω, is defined as:

$$\omega = T_{max}/N_p \quad (8)$$

where N_p is the yield force.

During the prequalification loading protocol, the factor is in the range 1.17-1.23, less than the maximum allowed value, 1.3 (ANSI/AISC 341-10 2010). The ω factor ranged between 1.35 and 1.66.

The starting direction of the loading protocol (tension/compression) did not seem to influence notably the response of the specimens. Individual observations per BRB typology are given below.

The four specimens of type A (BRBs with milled rectangular core, Fig. 6) designed for $N_{cr}/N_p \geq 3$ (CR73 and CR33) had a stable cyclic response during the qualification part of the protocol, fulfilling the P100-1/2013 (2014) and ANSI/AISC 341-10 (2010) qualification criteria. The cumulative inelastic deformation, *CID*, exceeded 330 times the yield Δ_{by}. The response was stable also during the extended protocol, but the maximum β value increased from 1.23 to 1.49. This is attributed to unsymmetrical deformations of the core at large amplitudes (see section 6.3).

The CR73 specimens (with the resistance of 700 kN) sustained a very large number of cycles (25), as well as *CID* of 1250 times the Δ_{by}. Ultimate strains of 4.53-5.20% were attained. The failure took place by fracture of the core in tension (Fig. 8).

One of the specimens designed for $N_{cr}/N_p = 1.5$ (CR71), fulfilled the qualification protocol but buckled in the first compression cycle of $2.5\Delta_{bm}$ (Fig. 10). The second one failed to complete the qualification protocol, buckling in the cycles of $2\Delta_{bm}$. Nevertheless, both specimens achieved *CIDs* larger than $200\Delta_{by}$.

(a) Front view (b) Side view (c) BRB-to-gusset lower connection view

Fig. 10 Failure mode of BRBs designed for $N_{cr}/N_p = 1.5$

(a) BRB Type A: specimen CR73-2

(b) BRB Type B: specimen CS73-2

Fig. 11 Uncovered BRBs after tests

The four specimens of type B (BRBs with square as-rolled core, Fig. 7) had a stable cyclic response, with β values ranging from 1.19 to 1.23 and *CIDs* of 349-459 times Δ_{by} during the qualification protocol. However, one of the specimens (CS73-1) failed to complete the last cycle, and consequently the qualification criteria. This is attributed to the large misalignment of the core extension plates. It is also noted that the measured yield strength of the CS73 specimens did not respect the specified steel grade. During the extended part of the protocol, ultimate strains of 3.88-4.64% were attained (smaller than for type A specimens due

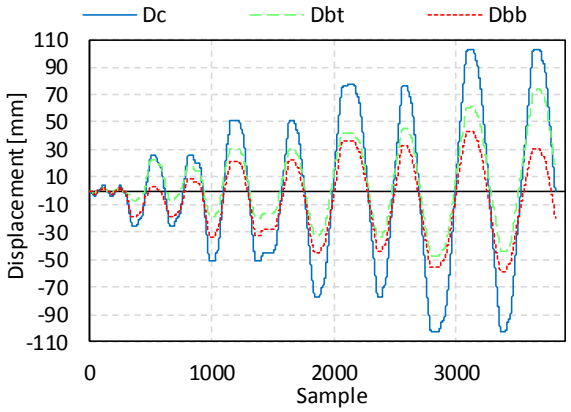

Fig. 12 Evolution of displacements D_{bb}, D_{bt} and D_c for the CS73-2 specimen

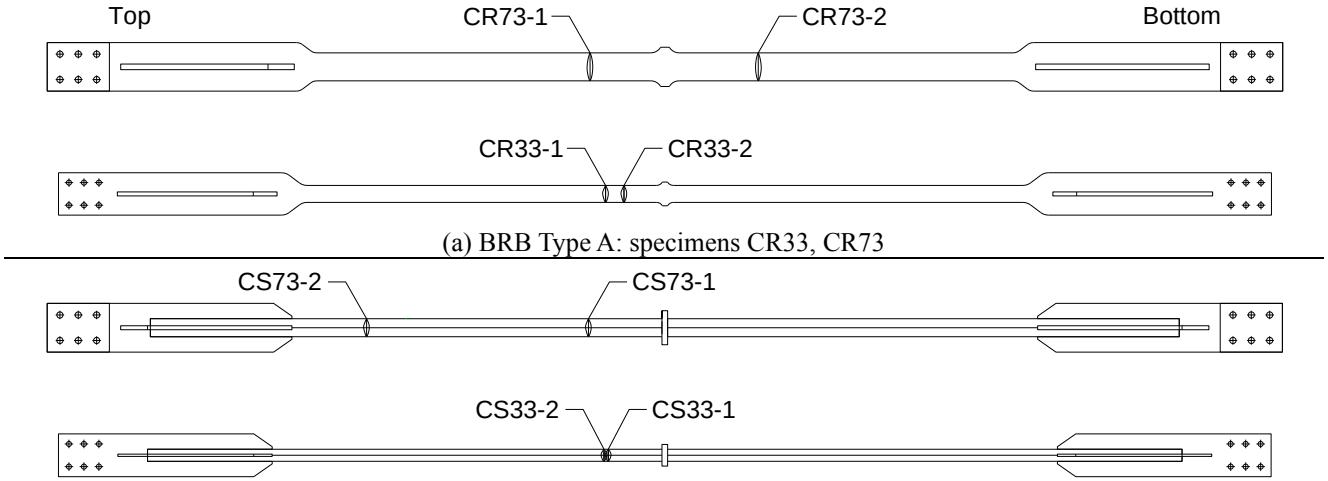

(a) BRB Type A: specimens CR33, CR73

(b) BRB type B: specimens CS33, CS73

Fig. 13 Failure position for BRBs designed for $N_{cr}/N_p = 3.0$

to longer core plastic zone). The failure took place by fracture of the core in tension.

6.3 Sizing of longitudinal gap

Visual examination of the tested BRBs was performed after uncovering the core and removing the acrylic tape. Fig. presents two representative specimens (CR73-2, CS73-2) per BRB typology, which failed by core fracture during tensile loading. Analysing the core-to-concrete interface, in the case of CR743-2 specimen, see Fig. (a), eight distinguished friction zones (dark spots) per half plastic zone length can be observed. In the case of specimen CS73-2, the friction zones per plastic zone length cannot be clearly distinguished, due to a stockier ross-section. In both cases, significant core-to-concrete interaction is observed near the transition zones. No damage to the concrete infill was observed for both specimens.

Fig. 13 presents the positions where the core fractured for the specimens which have the BRM designed for $N_{cr}/N_p = 3.0$. It needs to be noticed that welding of BRBs type B did not affect their cyclic performance since no fracture took place in or near the welding. It can be observed that all cores, except for the core of specimen CR73-2, fractured in the top part of the plastic zone, with respect to the position of the BRB in the experimental setup. Except for the specimen CS73-2 whose fracture position is rather close to the transition zone, in the case of all the other specimens the fracture position is close to the stopper. The failure positions from Fig. 13 suggest that the top part of the core plastic zone experienced larger deformations during the tensile phases of the cyclic loading than the bottom part, causing the fracture to take place in the top segment of the core of almost all BRBs. This aspect is confirmed by analysing the time-history of the displacements between the tube and the ends of the core (D_{bb} and D_{bt}), in comparison to the core deformation (D_c), see Fig. 12. It can be observed that during the tensile phase

the top segment of the core undergoes larger deformations than the bottom part, while during compression phase the bottom segment is undergoing larger deformations.

The non-symmetrical deformations in the top and bottom segments of the core affects the design of the longitudinal gap that allows the free movement of the core under compression cycles. To quantify this effect, maximum deformation ratios in the top (R_t) and bottom (R_b) parts of the core were determined for the 2.0 Δ_{bm} cycles

$$R_t = D_{bt}/D_c \tag{9}$$

$$R_b = D_{bb}/D_c \tag{10}$$

Maximum deformation ratios R_t and R_b are summarized in Table 5. Ideally, for a symmetrical response, both rations would be equal to 0.5. For all except one specimen, the deformation ratios in the top segment of the core are larger in tension (R_t = 0.52-0.72), while in the bottom part of the core the deformation ratios are larger in compression (R_b = 0.53-0.60). The longitudinal gap L_G (see Fig. 2) depends on the deformation in compression, whose maximum value was recorded at the bottom part: R_b = 0.6. This would require a longitudinal gap of at least $0.6\delta_{Ed}$. The design of the longitudinal gap L_G of a BRB is proposed to be determined slightly more conservative

$$L_G \geq 0.7\delta_{Ed} \tag{11}$$

where δ_{Ed} is the design deformation of the core.

If the longitudinal gap is designed assuming symmetrical response of the top and bottom core segments, the gap is insufficient, which results in the transition segment of the core coming longitudinally into contact with the concrete infill at one of the core ends. This leads to an increase in the compression force adjustment factor (β), as occurred for some specimens (e.g. CR33-2, Fig. 6) at the 2.5Δ_{bm} cycles.

6.4 Connection response

A typical response of the bolted BRB-to-gusset connection is shown in Fig. 14, where a pronounced pinching effect can be observed, due to the fact that the connection is not slip-resistant. Total deformation in a connection is the sum of slipping and bearing deformations of bolt in bolt holes.

Table 5 Maximum deformation ratios R_t and R_b

BRB ID	R_t		R_b	
	Tens.	Compr.	Tens.	Compr.
CR33-1	0.59	0.43	0.46	0.60
CR33-2	0.62	0.41	0.41	0.60
CR73-1	0.59	0.46	0.42	0.55
CR73-2	0.47	0.53	0.54	0.48
CS33-1	0.52	0.49	0.51	0.54
CS33-2	0.56	0.48	0.47	0.53
CS73-1	0.72	0.46	0.43	0.59
CS73-2	0.72	0.46	0.42	0.58

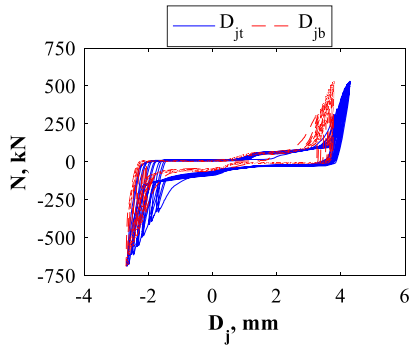

Fig. 14Connection deformations for specimen CS33-1

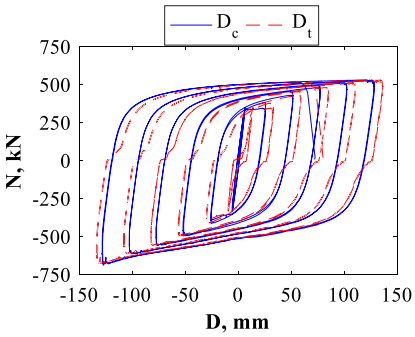

Fig. 15 Influence of bolted connection on the cyclic response of CS33-1 specimen

It can be observed that the connection deformation is roughly the same over the entire loading history, being governed by the slip.

The influence of the bolted BRB-to-gusset connection on the shape of the hysteretic loops of the BRB is presented in Fig. 15, where core (D_c) and total (D_t) BRB deformations are shown. The latter is determined as

$$D_t = D_c + D_{jt} + D_{jb} \tag{12}$$

The connection has a large contribution to the total deformations during small-amplitudes cycles. However, at large cycles, the effect of the connection is rather small. Consequently, bolted connections may affect the performance of the structure at the Serviceability Limit State, but would have a limited effect at the Ultimate Limit State. Therefore, it is recommended that slip-resistant bolted connections are used if serviceability criteria are critical.

6.5 Design parameters for qualified BRBs

To choose the optimal prequalified BRB solution, in addition to the performance parameters, two additional criteria were considered.

The first criterium refers to the possibility of adjusting the axial resistance of the BRB based on the tested yield strength of the steel plate or profile used to fabricate the core. BRBs of type A have the advantage of easy adjustment of the resistance since the core is obtained by

milling of a steel plate. BRBs of type B have less freedom in adjusting the resistance since the core is fabricated from a compact hot-rolled square steel profile, thus the resistance depends on the available size of the profiles.

The second criterium refers to the difficulty of the manufacturing process of the BRB, especially of the core, since the buckling restraining mechanism is similar for both BRB typologies. Fabrication of the core of BRB type B is much simpler, as the costly and time-consuming milling operation needed to manufacture the core of BRB type A is avoided. Also, because the core of BRB type B has a compact shape, it is less sensitive to bow imperfections in comparison with core of BRB type A, but careful alignment of the extension plates / stiffeners on the opposite ends of the core is required.

Based on the above-mentioned criteria (performance, adjustability and technology) it was concluded that the optimal BRB solution is the type A (BRB with milled rectangular cross-section core, having the BRM designed for $N_{cr}/N_p \geq 3.0$). The recommended values of strength adjustment factors for design of such BRBs are $\omega = 1.45$ and $\beta = 1.17$, while the ultimate core strain $\varepsilon_c = \pm 4\%$. The strength range of the qualified BRBs is 150-840 kN.

7. Conclusions

Ten full-scale buckling restrained braces of two different conceptual solutions were tested in view of prequalification for typical low-rise and mid-rise buildings for the seismic conditions of Romania. Most of the specimens performed well, with the stable hysteretic response, and ultimate core strains larger than 4%, sustaining the qualification protocol. Unsatisfactory performance was observed for specimens with lower strength of the buckling-restraining mechanism ($N_{cr}/N_p = 1.5$), or misalignments due to fabrication process (CS73-1 specimen). Based on the cyclic performance, technology and adjustability, the BRB solution with milled core encased in the concrete-filled tube was recommended as the qualified BRB for the strength range of 150-840 kN. The recommended values of strength adjustment factors for design of such BRBs are $\omega = 1.45$ and $\beta = 1.17$, while the ultimate core strain $\varepsilon_c = \pm 4\%$.

Gravity loading leads to unsymmetrical deformations in the two plastic segments of the core. Therefore, it is recommended that the length of each longitudinal gap is at least 70 % of the design deformation of the core.

Non-slip-resistant bolted BRB-to-gusset connections may affect the performance of the structure at the Serviceability Limit State, but would have a limited effect at the Ultimate Limit State. If serviceability criteria are critical, slip-resistant bolted connections are recommended.

Acknowledgements

The research leading to these results has received funding from the MEN-UEFISCDI grant Partnerships in priority areas PN II, contract no. 99/2014 IMSER: "Implementation into Romanian seismic resistant design practice of buckling restrained braces". This support is gratefully acknowledged.

References

ANSI/AISC 341-10 (2010), Seismic Provisions for Structural Steel Buildings, American Institute of Steel Construction; Chicago, IL, USA.

Black, C., Makris, N. and Aiken, I. (2002), "Component Testing, Stability Analysis and Characterization of Buckling-Restrained Unbonded BracesTM", PEER Report 2002/08. Pacific Earthquake Engineering Research Center, College of Engineering, University of California, Berkeley, USA.

Chao, C.C. and Chen, S.Y. (2009), "Subassemblage tests and finite element analyses of sandwiched buckling-restrained braces with a replaceable core", *STESSA 2009: Procc. of 6th International Conference for Behaviour of Steel Structures in Seismic Area,* Boca Raton, eds., Mazzolani F.M., Ricles J.M.and Sauce R., Philadelphia, Pennsylvania, USA.

Clark, P., Aiken, I., Kasai, K., Ko, E. and Kimura, I. (1999), "Design Procedures for Buildings Incorporating Hysteretic Damping Devices", *Proceedings of the 68th Annual Convention*, pp. 355–371, Structural Engineers Association of California, Sacramento, CA, September.

Dassault (2014), Abaqus 6.14 - Abaqus Analysis User's Manual, Dassault Systèmes Simulia Corp.

D'Aniello, M., Della Corte, G. and Landolfo, R. (2014), "Finite element modelling and analysis of 'All-Steel' dismountable buckling restrained braces", *Open Constr. Build. Technol. J.*, **8**, 216-226. DOI: 10.2174/1874836801408010216.

Della Corte, G., D'Aniello, M., Landolfo, R. and Mazzolani, F.M. (2011), "Review of steel buckling-restrained braces", *Steel Constr.*, **4**(2), 85-93. https://doi.org/10.1002/stco.201110012.

Della Corte, G., D'Aniello, M. and Landolfo, R. (2015), "Field testing of all-steel buckling-restrained braces applied to a damaged reinforced concrete building", *J. Struct. Eng.*, **141**(1), 1-11. https://doi.org/10.1061/(ASCE)ST.1943-541X.0001080.

EN 15129 (2010), Anti-seismic devices, European Committee for Standardization; Brussels, Belgium.

EN 1998-1 (2004), Eurocode 8: Design of structures for earthquake resistance - Part 1: General rules, seismic actions and rules for buildings, European Committee for Standardization; Brussels, Belgium.

Iwata, M. and Murai, M. (2006), "Buckling-restrained brace using steel mortar planks; performance evaluation as a hysteretic damper", *Earthq. Eng. Struct. D.*, **35**(14), 1807-1826. https://doi.org/10.1002/eqe.608.

Pandikkadavath, M.S. and Sahoo, D.R. (2016), "Cyclic testing of short-length buckling-restrained braces with detachable casings", *Earthq. Struct.*, **10**(3), 699-716.

P100-1/2013 (2014), Code for seismic design – Part I – Design prescriptions for buildings, Official Journal of Romania; Bucharest, Romania (in Romanian).

Sridhara, B.N. (1990), "Sleeved column as a basic compression member", *Proceedings of the 4th International Conference on Steel Structures & Space Frames*, Singapore.

Stratan, A., Voica, F., Marcu, D., Zub, C.I. and Dubina, D. (2015), "Design of buckling-restrained steel frames according to P100-1/2013", (in Romanian). *Proceedings of the 14th National Conference of Steel Structures*, Cluj-Napoca, Romania.

Stratan, A., Zub, C.I. and Dubina, D. (2018), "Experimental tests for pre-qualification of a set of buckling-restrained braces", *Key Eng. Mater.*, **763**, 450-457.

Tinker, J. and Dusicka, P. (2012), "Challenges in designing ultra-lightweight buckling restrained brace", Stessa 2012 – Mazzolani & Herrera (eds), Taylor & Francis Group, 569-575, London.

Takeuchi, T. and Wada, A. (2017), *Buckling-Restrained Braces and Applications*, The Japan Society of Seismic Isolation (JSSI), Jingumae Shibuyaku, Tokyo, Japan.

Tremblay, R., Bolduc, P., Neville, R. and DeVall, R. (2006), "Seismic testing and performance of buckling-restrained bracing systems", *Can J. Civil Eng.*, **33**, 183-198. https://doi.org/10.1139/l05-103.

Tsai, K.C., Lin, P.C., Wu, A.C. and Chuang, M.C. (2013) "Buckling restrained braces: research and implementation in Taiwan", *Proceedings of the Steel Innovations Conference 2013*, Christchurch, New Zeeland, February.

Uang, C.M., Nakashima, M. and Tsai, K.C. (2004), "Research and application of buckling-restrained braced frames", *Int. J. Steel Struct.*, **4**(4), 301-313.

Usami, T., Wang, C.L. and Funayama, J. (2012), "Developing high-performance aluminum alloy buckling-restrained braces based on series of low-cycle fatigue tests", *Earthq. Eng. Struct. D.*, **41(**4), 643-661. https://doi.org/10.1002/eqe.1149.

Vigh, L.G., Zsarnóczay, Á. and Balogh, T. (2017), "Eurocode conforming design of BRBF – Part I: Proposal for codification", *J. Constr. Steel Res.*, **135**, 265-276.

Watanabe, A., Hitomi, Y., Saeki, E., Wada, A. and Fujimoto, M. (1988), "Properties of brace encased in buckling restraining concrete and steel tube", *Proceedings of the 9th World Conf. Earthquake Engineering*, Tokyo, Japan, August.

Xie, Q. (2005), "State of the art of buckling-restrained braces in Asia", *J. Constr. Steel Res.*. **61**(6), 727-748. https://doi.org/10.1016/j.jcsr.2004.11.005.

Zub, C.I., Stratan, A. and Dubina, D. (in press), "Prequalification of a set of buckling restrained braces: Part II – numerical simulations", *Steel and Composite Structures*.

Zub, C.I., Stratan, A., Dogariu, A. and Dubina, D. (2018a), "Development of a finite element model for a buckling restrained brace", *Proceedings of the Romanian Academy Series A*, **19**(4), 581-588.

Zub, C.I., Stratan, A., Dogariu, A., Vulcu, C. and Dubina, D. (2018b), "Development of Two Types of Buckling Restrained Braces Using Finite Element Modelling", *Seismic Hazard and Risk Assessment*, Springer Natural Hazards, R. Vacareanu and C. Ionescu, eds., Springer International Publishing, 373-387, Cham, Switzerland.

CC